The Diffraction of Electromagnetic Waves on the Periodic
Heterogeneities and Its Use for Realization of Practical Technical
and Electronic Devices of Millimeter and Submillimeter Wavelength
Range [Текст] / H.V. Vorobiov, L. Vietzorreck, I.V. Barsuk, O.O. Rybalko
// Solutions and Applications of Scattering, Propagation, Radiation and
Emission of Electromagnetic Waves. — 2012. — Chapter 8. — P. 209-231

Chapter 8

The Diffraction of Electromagnetic Waves on the Periodic Heterogeneities and Its Use for Realization of Practical Technical and Electronic Devices of Millimeter and Submillimeter Wavelength Range

Gennadiy Vorobyov, Larissa Vietzorreck,
Ivan Barsuk and Aleksandr Rybalko

Additional information is available at the end of the chapter

http://dx.doi.org/10.5772/50694

1. Introduction

Among the open structures, which are used in millimeter and submillimeter (MSM) wave engineering, diffraction gratings (DG) made in different modifications (periodic metal and metal-dielectric structures (MDS)) are of primary importance along with open cavities and open waveguides. Such systems are basic in the design of electromagnetic oscillation sources and electronic components of different instrumentation of such wavelength range. If there is a diffraction of electromagnetic fields by DG, "two-act" wave transformation usually takes place. When homogeneous plane wave falls on the plane one-dimensionally periodic grating, scattered field can be considered as a spectrum of homo- and heterogeneous plane waves. In this case body (incident) plane wave is transformed into body (scattered) homogeneous plane and heterogeneous (surface) waves and, thus, "two-act" transformation occurs. This type of the boundary-value problems has been thoroughly studied in the work [1] and partly realized in the experiment [2]. In addition, processes of surface wave transformation of distributed sources into body waves by periodic heterogeneities are of special interest. Such phenomenon can be watched when an electron beam (EB) moves uniformly near the metal DG or periodic MDS. In this case self-surface field of the EB is scattered by DG and at least one of its harmonics is transformed into body wave of the diffraction radiation or Cherenkov radiation. It should be noted, that transformation of the surface wave of EB by DG into the diffraction radiation is also an example of the "two-act" diffraction process. In addition, phenomena, connected with the transformation of DG of the surface waves of a dielectric waveguide (DW), play a great role in

MSM engineering. In this case surface waves of a DW are transformed by the DG into surface waves of the DW or into body waves separated from them.

Multilinked quasi-optical systems in different modifications are very perspective in designing fundamentally new electronic devices and electronic components of instrumentation of MSM wavelength range including infrared waves. One should mentioned, that they are partly investigated by numerically-analytic methods in the approximation of constant current [1] and using the experimental modelling. It was determined that systems with MDS included in the open cavities structure can have qualitatively new properties [3] that makes it possible to propose high-frequency filters, frequency stabilizers, energy output devices from the volume of open cavities and new types of semiconductor oscillators on its basis. A possibility of the development of a Smith-Parcell amplifier was considered in paper [4].

Huge number of the previously proposed systems isn't accompanied with its complex research. This fact, therefore, makes the process of practical realization of new modifications of electronic device schemes and electronic components of MSM wavelength range on its basis very slow. So far existed numerical methods of optimization of the three-dimensional superhigh frequency structures [5, 6] enable to analyze effectively electrodynamic characteristics only of some multilinked quasi-optical system elements such as reflecting MDS. Meanwhile, a comprehensive solving problem of optimization of such structures requires the huge expenditure of computer time and computational power with usually ambiguous results in the end. That is why problems of development of the universal experimental facility, general technique of experimental modelling of the electromagnetic phenomena in multilinked quasi-optical systems and its realization for studying electromagnetic effects in complex quasi-optical systems using so far existed numerically-analytic methods, are very topical.

In the current work general electrodynamic characteristics of the multilinked quasi-optical system coupling elements have been determined on the basis of previous theoretical and experimental results in research of the simplest types of radiating system, formed by single-row DG, and using experimental modelling of transformation of the DW surface waves into body waves by two-row DG of different modifications. Schemes of practical microwave engineering devices have been suggested on basis of these characteristics.

2. An experimental setup and measuring technique

The use of periodic MDS formed by a strip metal grating on a dielectric layer is promising for both constructing extremely high-frequency electric vacuum devices (optical coupler and diffraction radiation generator [7, 8]) and integrated forms of various functional assemblies and devices, operating in MSM ranges, including the terahertz range [9]. In contrast to reflecting metal gratings, the MDS have a number of specific features related to a possibility of exciting spatial waves of Cherenkov, normal, and abnormal diffraction radiation, when an

http://dx.doi.org/10.5772/50694

EB moves along the MDS [1]. Therefore, it is necessary to have exhaustive information on electrodynamic characteristics of the DG and MDS, when they are used in various devices. Paper [1] presents a method for identifying properties of waves of the space charge of an EB traveling along a periodic structure, to the surface wave of the DW. This method has found a wide utility in simulating electrodynamic characteristics of various radiation modes of spatial waves on periodic MDS and on normal metal gratings. The setup for studying conversions of DW surface waves into body waves on normal metal gratings is described in [10]. However, its application for studying the MDS calls for modernization of the measuring part of the setup, taking into account special features of the analyzed object (possibility of the presence of body waves both in dielectric and outside).

Below, a universal setup that can be used for analyzing electrodynamic characteristics of both the MDS and traditional metal periodic structures is described. Results of test measurements are compared to the numerical analysis.

The complex experimental test bench for determining electrodynamic characteristics of periodic heterogeneities (MDS, strip and reflecting metal gratings), when they are excited by the DW surface wave, consists of two main modules (figure 1): (1) module for measuring waveguide characteristics (standing wave ratios (SWR), attenuation constants, etc.), and (2) module for measuring spatial characteristics of periodic structures (directional radiation patterns in the far-field zone and amplitude distributions of fields in the near-field zone). The module for measuring spatial characteristics includes the studied object, which is generally dielectric prism 1 with the strip DG 2 imposed on its side surface. Prism 1 is attached to the special adjusting unit intended to spatially orient it in the *x*-, *y*-, and *z*-directions with an error of ±0.1 mm. DW 3 joins in matching junctions 4, which through waveguides of specified sections, determined by the studied wavelength range, are mated with the waveguide characteristics recording unit and matched load 5. Depending on characteristics of the DW (phase velocity of the surface wave ν_{ph}) and MDS (strip grating 2 with period l and dielectric permittivity ε of prism 1), there are two possible modes of transforming the DW surface waves into body waves, which are excited with indices $n = 0, \pm1, \pm2, \ldots$ [1]. The main ones are shown schematically in figure 1 as directional radiation patterns (γ are the angles of radiation of the MDS-DW system, and ϕ are the angles of corresponding radiation harmonics in the free space after transmission through the dielectric prism).

The module for measuring spatial characteristics of the object consists of two versatile horn antennas 6, rotation axes of which pass in the *E*-plane through the radiation aperture and are brought into coincidence with the vertical axis of grating 2, and the rotation axis in the *H*-plane coincides with the DW longitudinal axis 3. This is intended to record radiation angles in interval $\phi = 10°–170°$ with error $\Delta\phi = \pm0.25°$, when the horns are mounted on special precision movable units and installed in the far-field zone, which is determined by the known ratio $z = a_m/\lambda$, where a_m is the maximal size of the antenna aperture, and λ is the radiation wavelength. In the course of measuring radiation patterns, the signal received by horn 6 arrived at input *Y* of the two-coordinate GP, and input *X* of the GP was connected to the rate-of-turn sensor of the receiving horn. Thus, when the movable antenna travels, the

directional radiation pattern is fixed on the GP, and, after conversion into digital form, it is used for the computer processing of the data received.

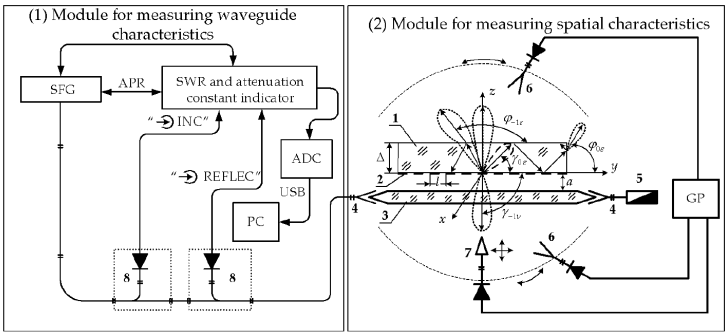

Figure 1. Block diagram of the experimental setup: (SFG) sweep-frequency generator, (APR) automatic power regulator, (ADC) analog-to-digital converter, (PC) personal computer, (GP) two-coordinate graph plotter. 1 — dielectric prism, 2 — strip DG, 3 — DW, 4 — matching junctions, 5 — matched load, 6 — horn antenna, 7 — probe, 8 — (DC) directional couplers, γ — radiation angles of the *MDS-DW system*, φ — angles of corresponding radiation harmonics in the free space after transmission through the dielectric prism, *x*, *y*, and *z* — spatial coordinates, Δ — thickness of the dielectric layer, *a* — distance between the DW and strip grating 2 (aiming parameter).

The amplitude field distributions along the axes of the radiating system are studied in the near-field zone ($z \approx \lambda$) by probe 7, made as a dielectric wedge ($\varepsilon = 2.05$), conjugated with the standard waveguide measuring section via the matching junction. Upon detecting, the signal from probe 7 arrives at the GP and is processed by the computer. Typical sizes of the probe of ~ (0.1–0.2)λ ensured minimal distortions of the fields during measurements. The surface field indication system was installed on the transportation carriage, and, in this case, samples in the *x*-, *y*-, and *z*-directions were obtained with an error of ~ 0.1 mm.

On the whole, all indication systems of spatial characteristics and studied object were placed on a single solid laboratory platform, illuminated by special precision adjusting units. This allowed us to orient the regular part of the DW with respect to the MDS plane with an error of ~ 0.1 mm and ensure the corresponding monitoring of the coordinates of measuring elements of the setup and studied object.

The module for measuring waveguide characteristics (figure 1) is based on a standard panoramic SWR and attenuation constant measurer, consisting of the SFG, SWR and attenuation constant indicator, and DC 8 with detector sections connected to corresponding connectors of the SWR indicator. Depending on the method of bringing the couplers into the measuring line, plots of either transmission gain or SWR were determined in the specified frequency range. The obtained results were processed by the designed ADC and arrived via the USB bus at the PC for further processing. The constant power level at the input to the studied object was kept by the APR, being the part of the panoramic measurer, and the minimal reflections at the DW output were ensured by inserting matched load 5 into the measuring

http://dx.doi.org/10.5772/50694

section (when absolute power levels were measured in the transmission line, standard wattmeters inserted directly into the measuring section instead of matched load 5 were used).

Procedure of performing measurements on the setup (figure 1):

(1) The matching of DW 3 with the module for measuring waveguide characteristics, which consists in reaching 1.1- to 1.2 SWR values for the specified frequency band by optimizing parameters of matching junctions 4. (2) Determination of the relative velocity of DW surface wave $\beta_w = \nu_{ph}/c$ (c is the velocity of light) and stray radiation level from matching elements 4. For this purpose, the calibration reflecting DG, characteristics of which are intended for radiation in the normal direction (angle $\gamma_{-1\nu}$ in figure 1) in accordance with the procedure [10], and indication system of fields in the far-field zone (horn antennas 6) are used. (3) Determination according to the procedure [1] of the optimal value of the aiming parameter a from the minimal distortion of directional lobes at the central frequency. (4) Determination of MDS and DW characteristics for the specified excitation modes of body waves in accordance with relationships of [1]. (5) Replacement of the calibration reflecting grating by the studied MDS. (6) Measurements of spatial MDS characteristics with the simultaneous automatic control of its waveguide characteristics.

The described experimental setup (figure 1) is implemented for a 53- to 80-GHz band, and this fact determined the selection, as a panoramic SWR and attenuation constant measurer, of a corresponding device and waveguide sections with a 3.6×1.8-mm^2 cross section. The fluoroplastic DW with a 5.2×2.6-mm^2 cross section permitted us to obtain relative phase velocities of the surface wave in interval β_w = 0.78–0.81 and to excite on the fluoroplastic MDS two main spatial radiation harmonics, namely, n = 0 (l = 1.17 mm) and n = –1 (l=3.07 mm). The performed test measurements of SWR, directional radiation patterns, and amplitude field distributions gave satisfactory results, as compared with the numerical analysis by the finite difference method [5]. Thus, in particular, directional radiation patterns of the studied MDS are shown in figure 2.

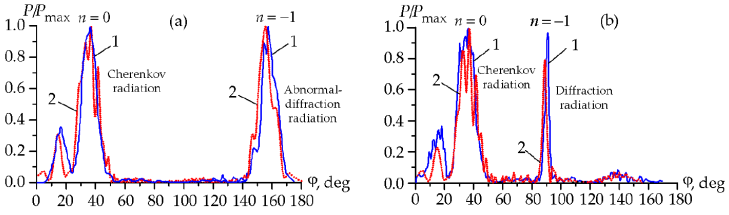

Figure 2. Typical directional radiation patterns of spatial waves on the MDS: (a) Cherenkov and abnormal-diffraction modes; (b) diffraction-Cherenkov mode. 1 — experiment, 2 — numerical simulation.

MDS parameters implemented in the experiment for three main operating modes of free-space wave excitation at the central frequency are given in the Table 1.

No	Operating mode of exciting spatial waves	*l* (mm)	*d* (mm)	*k*	*u*	β
1	Cherenkov *n* = 0 — in dielectric	1,17	0,39	0,30	+0,5	0,788
2	diffraction-Cherenkov *n* = 0, -1, -2 — in dielectric *n* = -1 — in free space	3,07	1,535	0,79	0	0,788
3	abnormal diffraction *n* = -1 — in dielectric	1,36	1,084	0,35	-0,8	0,598

Table 1. Parameters of the investigated MDS

The experimentally obtained data has been compared to the results of the numerical experiment based on solving Maxwell equations in a form of partial derivative using finite-difference approach and taking into account constitutive relations.

It follows from the given plots that the experiment satisfactorily correlates with the numerical analysis, and this, in turn, confirms serviceability of the described setup for studying electrodynamic characteristics of periodic structures belonging to a new class, i.e., planar MDS, which can find application in producing devices of MSM and terahertz wavelength ranges.

3. Practical devices of microwave technology and electronics

3.1. A quasi-optical directional coupler

The general principle of designing DC is to use two energy transmission lines coupled to each other [11, 12], along one of which the main power flow is transmitted; the auxiliary line is intended for interference and separation of forward and backward waves.

To date, depending on the imposed requirements, a great number of DC modifications are used in MSM wavelength measuring circuits.

The systems based on DW or dielectric planar waveguides [13] with distributed coupling, local coupling, and reemission into the secondary channel are the most close to the proposed DC.

In this work, the design of the DC based on two diffraction-coupled transmission lines with distributed radiation sources is studied, the sources being formed by periodic structures and DW placed along them. Figure 3 shows a general DC drawing and two possible reflector configurations, namely, plane-parallel and plane-cylindrical.

The basic DC section is formed from periodic structure 1, along the longitudinal axis of which DW 2 is placed at distance a. The second section is made similarly; it also consists of periodic structure 3 and DW 4. The periodic structures are applied on surfaces of flat and cylindrical mirrors with aperture *D*, the axes of which are placed in parallel at distance *H* and form a quasi-optical transmission line producing a beam of spatial waves. One of the

http://dx.doi.org/10.5772/50694

radiators of the system is installed so that it can move smoothly along axis *z*, changing distance *H* and correcting the phase characteristics of waves.

The principle of operation of the diffraction-coupled DC is based on exciting in-phase and antiphase spatial waves. As a result of the propagation of these waves along the longitudinal DC axis, the radiators exchange energies and some power is directed into the secondary channel. Results of theoretical and experimental studies of transformations of DW waves into spatial waves and of spatial waves into surface waves on periodic structures are described in detail in [1].

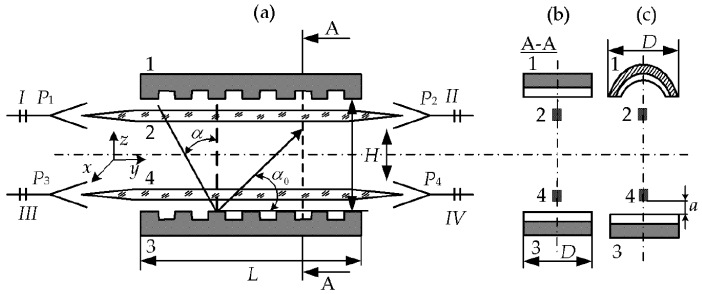

Figure 3. Schematic drawing of the design of the DC based on diffraction-coupled transmission lines: (a) cross section of components along the longitudinal axis; (b, c) cross section of components in the A–A plane at the (a) plane-parallel and (b) plane-cylindrical configurations of reflectors. 1, 3 — periodic structures, 2, 4 — DW, I–IV — arms of the DC, P_1 — power at the DC input, P_3 — power of the backward derived wave, P_2 , P_4 — transmitted powers.

Let us dwell on the special features of the wave processes in the proposed quasi-optical DC (figure 3). When the microwave signal is applied to input I, the delayed wave propagates in DW 2 and is scattered at periodic structure 1. In this case, a diffraction field arises, which is a superposition of plane waves. Some waves go into the DC volume at angles α as spatial waves, and the remaining ones are localized near the grating as slow harmonics propagating to the output of waveguide 2. The radiation angle of the spatial waves is determined by the relation [1]:

$$\alpha = \arccos\left(1/\beta_w + n/k\right) \tag{1}$$

where $\beta_w = v_w/c$ is the relative wave velocity in the DW; v_w is the phase velocity of the wave; n = -1, -2,… is the number of the spatial radiation harmonic; and $k = l/\lambda$ is the wave number (lis the period of the grating, and λ is the radiation wavelength). It is possible to obtain prevalence of one or another type of waves by selecting the radiator characteristics, namely, the period of the structure, the wave velocity in the waveguide, and impact parameter α.

The second excitation stage of the system in figure 3 is the incidence of the spatial wave formed at angle α on structure 3. As a result of diffraction, the complete field over the periodic structure consists of the incident and spatial harmonics of the scattered field. If $l<\lambda$/

(1+sinα), the zero spatial harmonic is only reflected from structure 3 at angle α_0=90°-α, while the remaining field is the superposition of surface spatial harmonics propagating along the grating with the phase velocities

$$v_f = kc / (n + k\sin\alpha) \tag{2}$$

When $v_f \approx v_w$, the delayed wave is also excited in DW 4 and is transformed into a spatial wave on periodic structure 3. When surface waves are successively transformed into spatial ones and spatial waves are transformed into surface ones, in-phase and antiphase waves are formed along the axis of reflectors of the DC and, as a result of their interference, part of the incident and reflected power is branched off to the secondary section.

The geometric sizes of the considered DC are selected from the inequalities [6] that specify the fulfillment of laws of ray optics in the double-mirror quasi-optical systemml:

$$\frac{d^2}{H\lambda} \ll \left(\frac{H}{d}\right)^2; l / \lambda \geq 10 \tag{3}$$

where H and L are the distance between the mirrors and their length, respectively, and d=D/2 is the aperture radius of the radiator mirrors (distance from the longitudinal axis of the system to the mirror periphery).

The fulfillment of the first inequality allows one to represent the field of the studied system as paraxial wave beams (figure 3), which are in many ways similar to a plane wave [14]. The second inequality minimizes the resonance phenomenon display along the longitudinal axis y. The structure period l is selected from (1) for specified values of λ, n, β_w, and α. The values of impact parameter $\alpha < \lambda$ are corrected experimentally by studying spatial characteristics of radiating systems, based on the criterion of the minimum parasitic DC effect on the field of the periodic structure.

When cylindrical mirrors with quadratic correction are used, the optimal values of their curvature radii, R, are in interval $2/R$ = 4÷6. This is attributed to the fact that the focusing action of the mirrors decreases at $2R/\lambda > 6$ and, for $2R/\lambda < 4$, the mirror aperture intercepts only part of the radiation of the periodic system–DW system.

We consider an example of selecting parameters of the DC and its components in frequency band f = 30÷37 GHz. As a source of the surface wave, a polystyrene waveguide with a cross section of 7.2×3.4 mm^2 was used. It provided for relative velocity $\beta_w \approx 0.9$ at the wavelength λ = 9 mm. The main lobe of the radiation pattern (n = -1) of the spatial wave was formed at angle $\alpha \approx 70°$, and, from relation (1), it corresponded to l = 11.5mm. The waveguide length L = 150 mm and radii of radiating apertures d = 30 mm ensured the fulfillment of conditions (3), and value R = 25 mm ensured the optimal focusing of the quasi-optical waveguide beam along the DC axis, when one of the mirrors was cylindrical (figure 3 (c)).

The experimental studies of the DC prototype were performed on the described above setup by measuring directional diagrams of the radiating systems and their near-zone fields and

http://dx.doi.org/10.5772/50694

also by measuring waveguide characteristics of both separate DC components and the system as a whole. The mechanical part of the setup allowed one to move DC radiators in three planes with an accuracy of ±0.1 mm and, by varying over wide ranges values a and H, to adjust the coupler according to optimal output parameter values.

As an example, the characteristics of the above design of the DC for two distances between the radiating mirrors are shown in figure 4.

It follows from these characteristics that, for the specified frequency interval, at distances between radiators H = 65 mm, the attenuation constant (P_4/P_2) values are in a 3- to 12-dB interval and the directivity factors (P_3/P_4) are in a 15- to 25-dB interval. It is possible to improve the DC output characteristics by correcting the phases of propagating waves, while H is varied; this is demonstrated by curves 2 in figure 4 ($P_4/P_2 \approx 3$–7 dB, and $P_3/P_4 \approx 30$ dB).

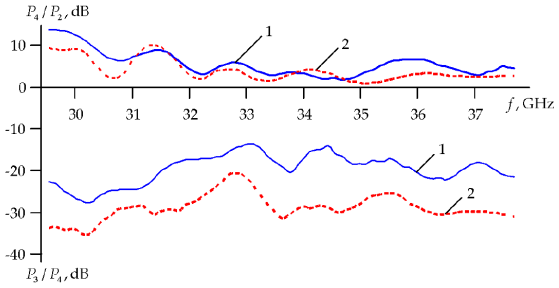

Figure 4. Characteristics of the coupler at (1) H = 65 and (2) 80 mm.

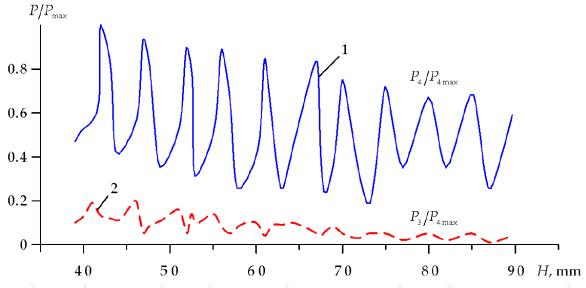

Figure 5. Relative power levels in the secondary channel as function of the distance between the mirrors. P_{4max} is the maximal power arriving at the secondary channel.

It is determined that the quasi-optical wave behavior of the studied system remains unchanged for H = (5–10) λ, for which inequality (3) is true.

Figure 5, in particular, illustrates the relative dependences of power levels $P_4/P_{4max} = f(H)$ and $P_3/P_{4max} = f(H)$, which are detected in arms IV and III, respectively (figure 3). It can be seen

from the plots that the optimal (from the viewpoint of decoupling the branched and reflected signals) values are H = 60–90 mm. At $H > 10\lambda$, the diffraction loss increases and the system becomes critical to the mirror alignment.

By comparing the characteristics of the described DC with couplers on coupled DW [15], the following conclusions can be drawn. The DC characteristics in the working frequency band Δf = 5 GHz are comparable with those of the coupler on the effect of the directional signal reradiation from the section of a sharp DW bend [15], the DC design being significantly simpler. In addition, this DC has two variants for correcting the transient attenuation (by changing impact parameter a and distance between radiators H), thus decreasing process requirements for manufacturing this system in the MSM wavelength range.

3.2. Quasioptical power dividers

In this subsection the results of studying the power divider (PD) design based on a two-row semi-transparent periodic structure with a distributed radiation source (main section) in the form of the DW, which is placed along its longitudinal axis are presented. In this system, the surface wave of the DW is transformed on periodic grids into spatial harmonics of body waves [16]. Figure 6 shows two PD modifications with longitudinal (Δd) and angular (ϕ) shifts of grid bars.

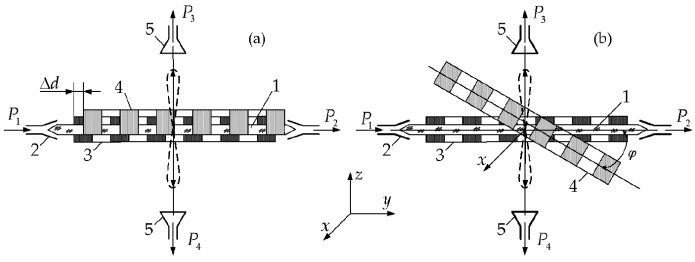

Figure 6. Embodiment scheme of the PD on two-row periodic structures: (a) with longitudinal Δd; (b) with angular φ shifts of grid bars. 1 — main section (DW), 2 — matching junctions, 3, 4 — grids, 5 — radiation receivers.

The PD contains DW 1, which is embedded into the main microwave section through matching junctions 2, grids made of bars 3 and 4, and radiation receivers 5. Grid 3 is fixed in position with respect to the y axis, and grid 4 is placed on the positioner that ensures either its linear movement along the y axis with accuracy Δd = ±0.01 mm or angular movement in the plane of the x, y axes with accuracy $\Delta\phi$ = ±1°. The radiation receivers operating in MSM wavelength ranges can be made, e.g., as horn or lens antennas and are intended for detecting the power diverted from the main section.

The principle of operation of these PD is based on transforming the DW surface wave into the spatial (body) wave, which is excited on the grids. The radiation power level of this wave can be regulated by changing phase relations of slow harmonics of waves excited on

http://dx.doi.org/10.5772/50694

the grids of the two-row structure when its bars are shifted or when the rotation angle with respect to the DW axis is changed.

We consider general features of wave processes in the described quasi-optical PD (see figure6). When the microwave signal with power P_1 is applied to the input of DW 1, the delayed wave propagates over its surface and scatters on grids 3 and 4. In this case, the diffraction field is formed, which is the superposition of plane waves. The part of these waves goes away into the free space (powers P_3 and P_4 extracted from the main power section) at angles γ_n in the form of spatial waves, and the remaining waves are localized near the grids in the form of slow harmonics propagating toward DW output 1 (power P_2 . The angle and conditions of emission of the spatial waves in the DW-grid system are determined from the relation [10]:

$$|\cos\gamma_n| = \frac{1}{k}\left(\alpha - \frac{2\pi n}{l}\right) \le 1 \tag{4}$$

where γ_n is the emission angle of the harmonic with index $n < 0$, 1 is the period of the grid, $k = 2\pi/\lambda$, and $\alpha = k - (2\pi n)/l$ is the propagation constant.

From equation (4), it follows that the waves with $n \ge 0$ and $|\cos\gamma_n| > 1$ are a spectrum of heterogeneous plane waves existing near the grid and propagating along the longitudinal axis of PD system with phase velocities $v_{ph} < c$, where the v_{ph} is the phase velocity of the wave, and c is the speed of light. For all remaining waves with indexes $n < 0$, the condition of their emission into the ambient space is met, which characterizes them as spatial (body) waves. By selecting appropriate parameters of the electrodynamic system and the surface wave propagating along the DW, it is possible to attain the predominance of one or another type of waves.

The geometrical sizes of the considered PD are selected from equation (4) when the fundamental ($n = -1$) spatial wave is emitted at angle $\gamma_{-1} = 90°$ to the plane of grids 3 and 4 and the latter are mirrored with respect to the DW axis ($\Delta d = 0$ and $\Delta\phi = 0°$). In this case, it is necessary to take into account the influence of bar thickness $2h$ on the radiation intensity [17]. The maximum bar thickness is determined as:

$$2h = N\frac{\lambda}{2} + d\frac{4}{\pi}\ln\sin\frac{\pi\theta}{2},\ (N = 1,2,...) \tag{5}$$

where d is the bar width, and θ is the relative distance between the grid bars.

In the grid with the optimal profile, somewhat smaller than the integer number of half-waves should be fitted in bar thickness $2h$. The correction for half-wave thickness $\Delta h = d\frac{4}{\pi}\ln\left(\sin\frac{\pi\theta}{2}\right)$ is equal for all harmonics and determined only by the geometrical parameters of the grid regardless of the wavelength and angle of emission. This correction is at maximum ($\Delta h_{max} = -0.23l$), when the slot width $\theta \cong 0.3$.

In addition, the intensity of the spatial waves in the considered systems can be regulated by the duty factor of the semi-transparent grids made of bars $u = \cos(\pi d/l)$ and sighting parameter a, which is the distance from the DW to the surface of the grids and determines the degree of relationship between the surface waves and heterogeneous waves of the grids.

The interval of the optimal value region of parameter Δd for the first PD modification (see figure 6(a)) was determined experimentally due to the absence of the theory of these systems. For the second PD modification (see figure 6(b)), the ranges of angles ϕ within which grid 4 is shifted with respect to grid 3 can be estimated from the limiting (critical) values of the angle of rotation of the single grid [10]:

$$\phi_{cr} = \arccos\left[\frac{1}{2}\left(\frac{k\beta_w}{n} - \frac{n\beta_w}{k} - \frac{k}{n\beta_w}\right)\right] \tag{6}$$

Hence, the surface wave mode occurs in the open structure of the DW and grid 4 at $\phi = \phi_{cr}$, and the further increase in ϕ results in the Bragg diffraction, for which $\phi_{Br} = \arccos\frac{N_B\beta_w}{2k}$, $N_B = 1,2,3,...$ is the order of diffraction. In this mode, the heterogeneous surface wave of the DW is transformed into the surface wave of the grid. The formed new surface wave propagates at an angle of (180°–ϕ) with the direction of the original heterogeneous wave. The degree of transformation of one wave into the other is determined by the longitudinal dimensions of the grid and the coupling between the DW and grid field.

As an example, let us select the parameters of the PD and their main elements in the four-millimeter wavelength range (f = 60–80 GHz). As a source of the surface wave, a fluoro-plastic waveguide with a 5.2×2.6 mm^2 cross section is used, which ensures the relative wave velocity $\beta_w = 0.788$ at wavelength $\lambda = 4$ mm. The main lobes of the radiation pattern (n=–1) of the spatial waves were formed at angle $\gamma = 90°$. According to equations (4) and (5), this corresponded to values $l = 3$ mm, $u = 0$, and $2h = 1$ mm. The grid aperture $D = 60$ mm and their length along the DW axis $L = 54$ mm ensured the meeting of the main quasioptic conditions [15].

The experimental studies of the PD prototypes (figures 6 (a), (b)) were performed in accordance with the described above procedure.

As an example, the amplitude (relative values P_3 / P_{3max}) and waveguide (transmission coefficients $K_{tr} = P_2 / P_1$) characteristics of the above PD are shown in figure 7. They indicate that it is possible to extract 80% of the power from the main section ($P_2 = 0.2P_1$) and divide it equally when the grids are placed symmetrically with respect to the DW ($P_3 = P_4 = 0.4P_1$) for the specified sighting parameter $a = 0.7$ mm.

The analysis of the plots in figure 7 shows that the power in the arm P_3 can be smoothly regulated either by shifting the bars or changing the rotation angle of grid 4 with respect to axis of grid 3. In this case, for the PD modification in figure 6 (a), it is expedient to select the $\Delta d/\lambda$ values in an interval of 0.2–0.4, in which the dependence of the radiated power is close to the linear one and has no resonance effects.

http://dx.doi.org/10.5772/50694

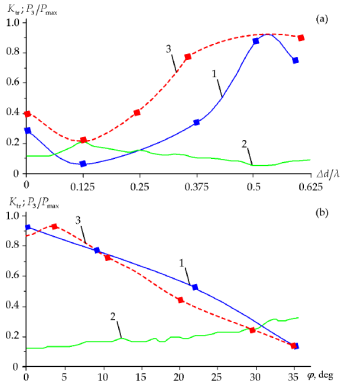

Figure 7. Amplitude and waveguide characteristics of the PD with (a) longitudinal and (b) angular shifts of grid bars with respect to the axis of the waveguide. 1 — relative power values P_3, 2 — K_{tr} values, 3 — calculated curve.

From the viewpoint of regulating and calibrating the emitted power P_3, the second PD modification is preferable (figure 6 (b)). Its amplitude characteristic is virtually linear for the selected angle interval ϕ = 0–35°. For both PD modifications, the standing-wave ratio values were 1.1–1.3 in frequency range f = 60–80 GHz. The characteristics shown in figure 7 were numerically simulated by the finite difference method [5], and the calculated results are illustrated in figure 7 by dotted lines 3. The comparison of the experimental results and numerical analysis indicates their correlation.

By analyzing the characteristics of the described PD, it is possible to make the following conclusions. In contrast to the waveguide analogs and PD on DW [15], the described PD possess wider functional capabilities, allowing one to divide the power coming from the main section into equal parts between two channels and smoothly regulate it in one of the output arms of the divider. In this case, the powers arriving at the output arms of the divider can be regulated by changing the sighting distance of the DW with respect to the grid surfaces. The presented PD can be also manufactured in the planar form if periodic MDS are used [11].

3.3. Possible variants of implementation of MSM radiation sources

Nowadays MSM microwave devices (backward-wave tubes, taveling-wave tubes, klystrons) with high level of output power are widely used in transmitting equipment of communication systems, radars and radio countermeasures devices. Thus, there is the rapid development in production of traveling-wave tubes with slow-wave structures as a chain of coupled resonators in different geometrical modifications [8], creation amplifiers based on the multielectron-beam tubes [18] etc. Axially symmetric EB as the main working element of such devices virtually defines their basic working parameters. Therefore, special attention is given to the improvement and optimization of electron-optical systems of MSM microwave devices.

As a rule, an optimization of electron-optical system parameters bases on the information about EB characteristics. Currently, because of the rapid development in computational re-

sources and approaches, different techniques of electromagnetic simulation based on various numerical algorithms are mostly used to get this information. Such approach allows avoiding carrying out time-consuming and expensive experiment. Usually modelling techniques consist of two stages: computation of electromagnetic fields of the investigated system and subsequent trajectory analysis of charged particles in these fields.

In the current subsection the example of the model of the three-electrode electron gun which is used in real microwave devices such as travelling-wave tube has been presented, the optimization problems of its operating modes and axially symmetric EB characteristics have been outlined.

Axially-symmetric EB, as a rule, is formed by three-electrode electron gun with converging optics and introduced into slowing-down system where it is focused by periodic magnetic field. The cathode is usually produced in the form of a core made of tungsten-rhenium blend with activated surface. The typical electrode configuration of axially symmetric electron-optical system is demonstrated in figure 8.

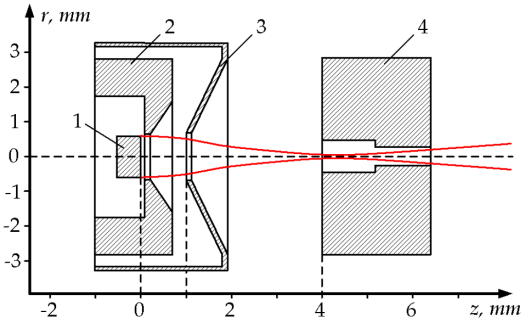

Figure 8. Scheme of electron-optical system of axially symmetric electron gun: 1 — hot cathode (U_k), 2 — focusing electrode (U_f), 3 — first anode (U_{a1}), 4 — second anode (U_{a2}).

The guns of such type allow forming EB with diameter of about 0.3mm in the crossover, the beam current of 1–25 mA with accelerating voltage 2000–6000 V. For numerical simulations the finite integration technique (in literature is known as FIT [19]) was chosen as the optimal numerical algorithm for analyzing the above mentioned systems.

The combination of electrode potentials, described in [20], was taken as the initial parameters with a beam perveance P = 0.045 mkA/V$^{3/2}$, the number of emitted particles N = 2965, average kinetic energy of electrons E_k = 5 eV with energy spread dE_k = ±0.33 E_k, maximal angular deflection α = ±10° from the axis of the system, that corresponds to the real guns of such type. Meanwhile, the emitting area has been defined as a perfectly plane surface with the uniform current density distribution.

http://dx.doi.org/10.5772/50694

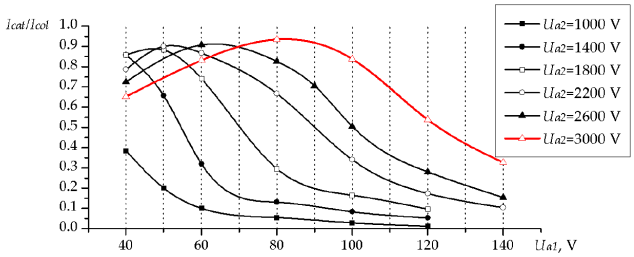

Figure 9. Coefficient of the EB passage with the different potential values U_{a1} and U_{a2}.

When simulation of the electron-optical system is carried out, the main parameter of optimality is the coefficient of EB passage. That is why in the first step of the optimization of the electron gun operating modes the research of a beam passage coefficient $K = I_{cat}/I_{col}$ was conducted, where I_{cat} and I_{col} are cathode and collector currents respectively. The simulation has shown that too high potential of focusing electrode ($U_f \approx$ -40V) impairs the passage of EB and causes unsatisfactory crossover position between two anodes of electron-optical system but not after the second anode. In addition, as the focusing electrode is placed in the immediate vicinity to the cathode surface the partial EB blocking effect is created and the kinetic energy of the emitted electrons is not high enough to overcome thus formed potential barrier. This blocking effect decreases considerably an EB passage ratio and disturbs beam laminarity. Changing the potential of the focusing electrode might partly solve mentioned problems. When U_f is decreased to zero potential the beam crossover is shifted to the region of the second anode transit channel. In this case the diameter of the crossover decreases and the passage of EB with U_f = -10÷0V might reach 93-95%. Thus, to avoid any impact of the focusing electrode on the cathode edge U_f = 0V was taken as the most appropriate for the experimental research, filament current of the tungsten- rhenium (W-Re) cathode for the whole set of measurements was constant — 0.7 A.

Experimental measuring results have shown that the coefficient of the EB passage increases with increasing U_{a2} nd riches the value of K = 0.934 with U_{a2} = 3000V, that corresponds to the current value I = 9.1 mA. However, further increasing of the U_{a1} and U_{a2} potentials stimulates electron emission and causes rapid growth of the cathode current (I_{cat} > 15 mA). This, in turn, leads to the strong heating of the gun elements, bombarded by electrons, which considerably disturb the consistency of the device operation and causes different measurement errors.

Figure 9 shows that the coefficient K reaches its maximum value at the accelerating potentials of U_{a1} = 80 V and U_{a2} = 3000 V. Thus, such electron-optical system operating mode can be considered as the optimal for the passage of the EB.

Besides the information about the electron deposition on the gun electrodes, which allows carrying out a preliminary analysis of its operating modes, the EB quality parameters (such as type of a particle distribution in the cross-section, laminarity, spread of the velocity transverse components etc.) are also very important. In the current work root-mean-square emittance (statistical emittance) was used to describe such characteristics:

$$\varepsilon = \left(\langle x^2\rangle \cdot \langle x'^2\rangle - \langle x \cdot x'\rangle^2\right)^{1/2} = \left(\langle x - \langle x\rangle^2\rangle \cdot \langle (x' - \langle x'\rangle)^2\rangle - \langle (x - \langle x\rangle) \cdot (x' - \langle x'\rangle)\rangle^2\right)^{1/2} \quad (7)$$

where

$$x' = \frac{v_x}{v_\perp},\ \langle x\rangle = \frac{1}{N}\sum_{n=1}^{N} x_i \quad (8)$$

It should be noted, that formula of this type in contrast to other definitions makes it possible to express an EB emittance in a simple numerical form. In addition, we do not find it reasonable to consider a normalized beam emittance in this case because of short drift duct and low accelerating potentials of the system (EB is not relativistic) [21].

The calculated emittance with the maximal passage of the EB at a distance of 10 mm from the cathode made up ε_x = 1.71 mrad·mm and ε_y = 1.85 mrad mm in x- and y-directions respectively, the beam diameter — D = 0.8 mm.

However, as the numerical experiments to study transversal electron dynamics (figure10 (a)) has shown, value of the emittance can be decreased by variations of the potential U_{a1}.

The analysis of two-dimensional diagrams of the transversal emittance has demonstrated that the increase of the U_{a1} to 110 V considerably disturbs the beam laminarity (figure10(b)) while its decrease improves the EB quality (type of the diagram corresponds to the perfectly divergent beam) with slight growth of its diameter ($D \approx 0.8$ mm). On the basis of the analysis of experimental and numerical simulation results the optimal operating mode with the potentials U_{a1} = 60 V и U_{a2} = 3000 V has been chosen. It allows getting the passage of the EB at the level of $K \approx 0.85$ with transversal emittance values ε_x = 1.67 mrad·mm and ε_y=1.76 mrad·mm.

Development of high-resolution sensitive elements for terahertz frequency bandwidth is an actual problem due to a number of existing international projects of radio astronomy as well as the projects with the objective of studying the Earth atmosphere. The basic issues of arrangement of receivers in the given bandwidth are solved by application of solid-state heterodyne oscillation sources and the mixers based on the effect of electron heating in the superconductor (Hot Electron Bolometer) because such mixers have no competition analogs in this bandwidth. By now these mixers have been successfully realized at the frequencies of the order of 3 GHz. However, several research projects are related to development of the mixers optimized for higher frequencies; e.g. within the framework of the SOFIA project it is developed a heterodyne receiver for 4.8 THz. Principal opportunity for creation of the mixer for the given bandwidth is shown in the paper [22] where the method of electron and photo lithography is applied for its realization. As an example, figure 11 provides photos of the central part of the mixer obtained with the scanning electron microscope.

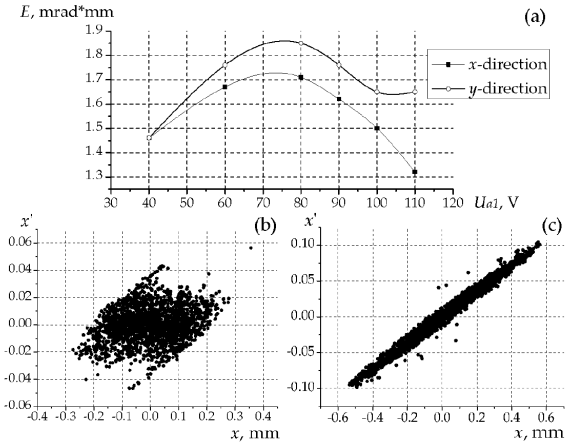

Figure 10. Dependence of EB emittance on the U_{a1} potential: (a) numeral values in *x*- and *y*-directions; (b), (c) two-dimensional diagrams for U_{a1} = 110 V and U_{a1} = 40 V, respectively.

The mixers were made of NbN films with the thickness of 2 to 3.5 nm upon a silicon substrate with a MgO buffer sublayer and possessed the temperature of superconducting transition of 9 to 11 K. The best value of the noise temperature of the receiver on the basis of the electron heated mixer amounted to 1300 K and 3100 K at the heterodyne frequencies of 2.5 and 3.8 THz correspondingly.

In the radio astronomy devices and tools the preference is given to solid state heterodyne sources within the terahertz band due to their small dimensions, low weight and power consumption requirements, despite low output power level, which is not exceeding 1 μW at the frequency of 2 THz that to a significant extent complicates the problem of development of mixers for a low level of output power. Thus, there still remains actual the problem of realization of low-voltage electrovacuum oscillation sources within the terahertz wavelength band possessing higher values of power levels as compared to those of solid state oscillators.

By the present time this problem can be solved by means of using in the vacuum electronics of planar periodic MDS [1, 11]. Block diagrams of such devices that could be realized on the basis of the above described technologies and new types of dielectrics with larger values of dielectric permeability and low loss values at high frequencies [23], are provided in figure12.

Block diagram of the oscillator in figure 12(a) suggests modulation of the EB upon a backward wave of the periodic structure (position 2) with subsequent excitation of the Cherenkov oscillation harmonic in MDS (position 3). Within the oscillator in figure 12(b) it is applied the mode of abnormal diffraction oscillation, which is realized at substantially less values of accelerating voltages of the electron flux compared to those of the Cherenkov oscillation harmonic.

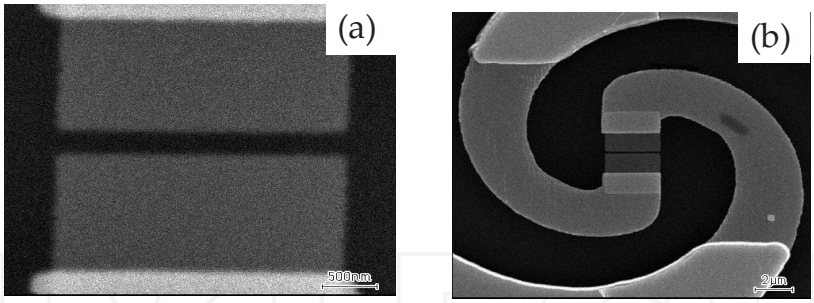

Figure 11. Image of the helix (a) and of the central part of the helix with the NbN bridge (b) obtained with the scanning electron microscope [22].

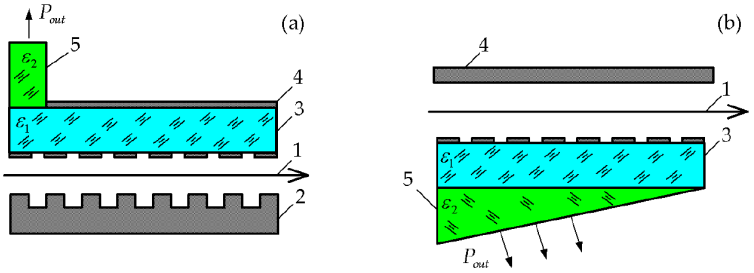

Figure 12. Block diagrams of terahertz frequency band electrovacuum oscillation sources.1 — EB, 2 — periodic structure, 3 — MDS with diffraction strip-like grating, 4 — screen (mirror), 5 — energy output device.

At practical realization of the above block diagrams of sources of oscillation it is necessary to solve a set of problems related to the technology of manufacturing of main units of the device – the electrodynamic system, the low-voltage source of electrons and the focusing magnetic system. The above considered technological processes – like, for instance, nano die forming – eliminate all problems related to manufacturing of both reflecting and ribbon (applied upon the dielectric layer) DG with the micron period.

Oscillator schemes presented in figure 10 are the ideological continuation of the so far developed low-voltage backward-wave tube with multi-row slow-wave structures [8, 24]. A schematic view of a low-voltage orotron based on parallel MDS and three EB are shown in figure 10 (a). The calculated MDS parameters have been determined for EB radiation at the angle of 90°. The diagram of a backward-wave tube based on an anomalous diffraction radiation for MDS is shown in figure13 (b). The arrows show the direction of wave radiation on the MDS.

http://dx.doi.org/10.5772/50694

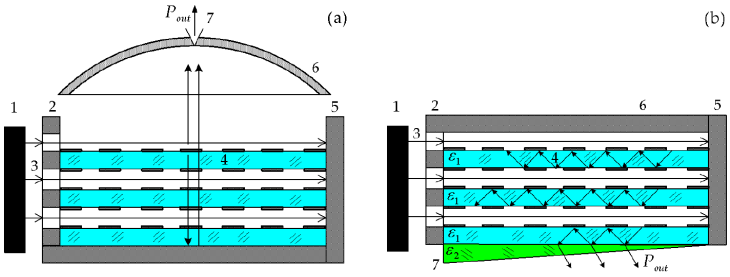

Figure 13. Schematic view of low voltage vacuum devices employing multi-linked MDS:(a) orotron, (b) backward wave oscillator. 1 — cathode, 2 — anode, 3 — EB, 4 — planar periodic MDS, 5 — collector, 6 — mirror, 7 — output port.

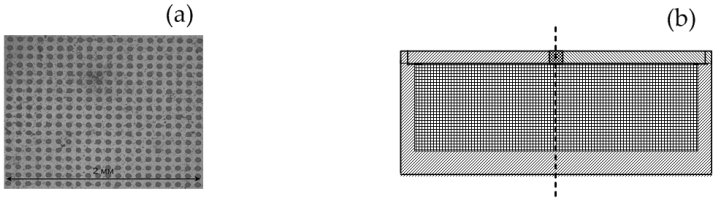

Figure 14. Microphotographic images of the field cathode surface [27] (a) and block diagram of the "slot" L-cathode device [28] (b).

The analysis of parameters of the discussed electrodynamic systems [11] and devices demonstrated in figure 13 shows that the DG/MDS or multi-row systems on basis of MDS at acceleration voltages $U \approx 1000$ V and $\varepsilon_r = 100$ (ceramics based on titanium oxide) can be realized for a wave length range from 1mm to 0.1 mm and periods lfrom 64 μm to 4 μm. Currently the fabrication technology for such structures is mature and has been used for fabrication of multiple parallel slow-wave structures in backward-wave tube. The fabrication technologies include electro-erosion machining, cold forming, photolithography, electron and x-ray lithography, vacuum and plasma deposition. The fabrication of slow-wave structures of vacuum electron tubes requiring nanoscale precision is performed by ion beam lithography [25] in combination with nanoforming [26].

The research conducted in [1] indicates that in order to realize the described devices in submillimeter and infrared wave ranges, an EB should be as thin as 0.04 mm. Nowadays the practical realization of such EB is possible using array type or slot type L-cathode, which allow getting uniformly distributed and stable electron emission with high current density at comparatively low field intensity.

The matrices of field emission cathodes possess the preset geometrical dimensions (diameter, step), they allow elimination of the screening effect and obtaining of homogeneous upon the

surface and stable in time electron emission with the average current value of 40 μA from a separate cathode at relatively low electric field intensity values. The cathode represented in figure 14 (b) includes the cylinder container filled with a stock of the substance that decreases the output operation of the operating surface, which is represented by a continuous row of micro-elements forming up a "slot" L-cathode. Experimental results obtained while pilot testing of those cathodes at IRE NAS of Ukraine proved the opportunity for obtaining of such electron fluxes with high-value current density at not high values of accelerating voltages.

4. Conclusions

In the current work the results of development of the experimental setup and procedure for measuring electrodynamic characteristics of planar periodic MDS, which can be used for manufacturing practical equipment operating in MSM and terahertz wavelength ranges are presented. Serviceability of the setup is checked by comparing the waveguide and spatial characteristics obtained experimentally and by numerical methods in a 4-mm wavelength range. A circuit and principle of operation of DC based on diffraction-coupled transmission lines, the emitting apertures of which are formed from periodic structures and DW has been proposed on the basis of the conducted research.

The experimental studies of the coupler prototype in a 30- to 37-GHz band have shown that the coupling on spatial waves allows one to obtain transient attenuation values in a 3- to 20-dB interval at a ~ 30 dB directivity, this being roughly in conformity with similar characteristics of a coupler on DW. The main advantage of the described DC is that it is possible to correct its characteristics over wide ranges by changing the distance between the emitting apertures.

Circuits and principle of operation of quasi-optical PD based on two-row periodic structures, formed by grids of metal bars and a DW placed along their longitudinal axis, have been proposed and described as the second example of realization of described above characteristics. The experimental studies of PD prototypes in a frequency range of 60–80 GHz have shown a possibility of regulating the emitted power level in the main divider arm by changing longitudinal and angular coordinates of the two-row periodic structure, which can be used for designing quasi-optical attenuators.

The example of the model of the three-electrode electron gun of travelling-wave tube has been described, the optimization problems of its operating modes and axially symmetric EB characteristics have been outlined.

In addition, studied properties of electrodynamic diffraction characteristics of the surface waves on periodic heterogeneities can be realized in implementation of radiation sources on the Smith-Parcell effect.

Work is supported by the governmental programme No0112U001379.

Author details

Gennadiy Vorobyov[1*], Larissa Vietzorreck[2], Ivan Barsuk[1] and Aleksandr Rybalko[1]

*Address all correspondence to: g.vorobyov@sumdu.edu.ua

1 Sumy State University, Sumy, Ukraine

2 Technische Universität München, München, Germany

References

[1] Shestopalov, V.P. (1991). *Diffraction radiation oscillators*, Kyiv, Naukova Dumka.

[2] Vorobjov, G., Shulga, Yu., & Zhurbenko, V. (2011). Quasi-optical Systems Based on Periodic Structures. *Zhurbenko V. (ed.) Electromagnetic Waves*, Rijeka, InTech, 257-282.

[3] Vorobjov, G. S., Petrovskii, M. V., & Krivets, A. S. (2006). Possible applications of quasioptical open resonant metal-dielectric structures in EHF electronics. *Radioelectronics and Communications Systems*, 49(7), 38-42.

[4] Vorobjov, G. S., Tsvyk, A. I., Krivets, A. S., Shmatko, A.A., & Petrovsky, M. V. (2003). The Smith-Pursell Effect Amplification of the Electromagnetic Waves in a Open Waveguide with a Matal-Dielectric Layer. *Telecommunications and Radio Engineering*.

[5] Bankov, S.E. (2004). *Analysis and optimization of microwave three-dimensional structures with HFSS.*, Moscow, Solon-Press.

[6] Sirenko, Yu. K., Strom, S., & Yashina, N. P. (2007). Modeling and Analysis of Transient Processes in Open Resonant Structures: New Methods and Techniques. New York, Springer.

[7] Bratman, V. L., Glyavin, M., Yu, , Kalynov, Yu. K., Litvak, A. G., Luchinin, A. G., Savilov, A. V., & Zapevalov, V. E. (2010). Terahertz Gyrotrons at IAP RAS: Status and New Designs. *Journal of Infrared, Millimeter and Terahertz Waves* [8], 8-934.

[8] Yakovenko, V.M. (2007). *Vacuum devices millimeter waves*, Sevastopol, Weber.

[9] Federici, J., & Moeller, L. (2010). Review of terahertz and subterahertz wireless communications. *Journal of Applied Physics* [107], 107-1063.

[10] Shestopalov, V.P. (1985). *Physical basis for millimeter- and submillimeter-wave equipmen. 1Open-type structures)*, Kyiv, Naukova Dumka.

[11] Vorobyov, G. S., Petrovsky, M. V., Zhurba, V. O., Ruban, A. I., Belous, O. I., & Fisun, A. I. (2007). Perspectives of application of new modifications of resonant quasi-optical structures in EHF equipment and electronics. *Telecommunications and Radio Engineering*, 66(20), 1839-1862.

[12] Xiao-Ping, Chen., & Ke, Wu. (2008). Substrate Integrated Waveguide Cross-Coupled Filter With Negative Coupling Structure. *Microwave Theory and Techniques, IEEE Transactions on Microwave Theory and Techniques*, 56(1), 142-149.

[13] Demydchik, V.I. Microwave electrodynamics Minsk Universitetskoe (1992). .

[14] Weinstein, L.A. (1966). *Open resonators and open waveguides*, Moscow, Sov. Radio.

[15] Valitov, R.A. (1969). *Submillimeter-wave equipment*, Moscow, Sov. Radio.

[16] Quan, X., Kang, X., Yinghua, R., & Jun, T. (2011). 3dB power splitter design based on coupled cavity waveguides. *International Journal for Light and Electron Optic*, 122(2), 156-158.

[17] Shestopalov, V.P. (1976). *Diffraction electronics*, Kharkiv, Kharkiv UniversityPublishers.

[18] Sinicin, N. I., Zakharchenko, Y. F., & Gulyaev, Y. V. (2009). A new class of high-power low voltage multipath TWT elated to chains multiple-Resonators with a transversely-extendedtype of interaction for airborne radar and communication systems the short-millimeter waves. *Jornal of radioelectronics*, 50(10), 46-51.

[19] Weiland, T.A. (1977). Discretization Method for the Solution of Maxwell's Equations for Six-Component Fields.Electron. *Commun. (AEU)*, 31(3), 116-120.

[20] Belousov, Ye. V., Vorobyov, G. S., Korg, V. G., Pushkarev, K. A., & Chaban, V. Y. (1992). Experimental investigation of the static parameters axisymmetrical electron beams of small diameter. *Recent developments in applied physics*, 2(1), 87-100.

[21] Braun, Ian. G. (1998). *The physics and technology of ion sources*, New York, A Wiley and Interscience Publication.

[22] Finkel, M. I., Maslennikov, S. N., & Goltsman, G. N. (2005). Superheterodyne receivers with superconducting THz mixer on electronic heating. Trans. Higher Education. *Radio Physics*.

[23] Nanasheva, Ye.A., Trubitsina, O. N., Kartenko, N. F., & Usov, O.A. (1999). Ceramic materials for microwave electronics. *Solid State Physics*, 41(5), 882-884.

[24] (2002). *Vacuum Microwave Electronics: Collection of reviews*, Nizhny Novgorod, Institute of Applied Physics.

[25] Watt, F., Bettiol, A. A., van Kan, J. A., Teo, E. J., & Breese, M. B. (2005). Ion beam lithography and nanofabrication. *International Journal of Nanoscience*, 4(3), 269-286.

[26] Ansari, K., van Kan, J. A., Bettiol, A. A., & Watt, F. (2006). Stamps for nanoimprint lithography fabricated by proton beam writing and nickel electroplating. J. Micromech. *Microeng.*, 16-1967.

[27] Solovey, D. V., Sakharuk, V.N., & Novitsky, A.M. (2009). *19th International Crimean Conference "Microwave Equipment and Telecommunication Technologies CriMiCo 2009 September*, 14-18, Sevastopol National University, Sevastopol, Ukraine.

[28] Belousov, Ye. V., Zavertannyi, V. V., & Nesterenko, A. V. (2006). Diode electron gun with a slot L-cathode. *Radio Physics and Electronics,* 11(2), 275-280.

INTECH

INTECH